Catalogue of C200 chopped observations

Attila Moór, Péter Ábrahám, Csaba Kiss

2006

Contents

1 Introduction and General Principles

The release of the final version of the ISOPHOT Off-Line Processing software (OLP V10.0) and the generation of the ISO Legacy Archive closed the main period of ISOPHOT calibration in 2002. In this phase the calibration work focused on general instrumental effects with impact on several or all observing modes, and the correction algorithms developed were as general as possible in order to ease the software implementation. The photometric quality reached with the OLP is documented in the Scientific Validation Report (Klaas et al., 2002b) and in the ISOPHOT Calibration Accuracies Document (Klaas et al., 2002a).

In a very general calibration approach, however, specific problems of individual observing modes (or submodes) might be overlooked or ignored. In order to improve further the photometric accuracy of ISOPHOT our strategy is to carry out more specific calibration investigations focusing on particular problems of well-defined homogeneous data sets, and to work out dedicated correction algorithms which are not necessarily applicable to other data sets. We adopt the following general scheme for the analysis of a selected well-defined ISOPHOT observing mode or submode:

1. Collect from the Archive all observations performed in the selected observing mode;
2. Identify all objects which can be used as secondary photometric standards;
3. Process the measurements of identified standard objects using an OLP V10.0-compatible data reduction method;
4. Search for any systematic trend in the distribution of the [Measured-Predicted] residual flux densities;
5. Investigate the physical reason behind the observed trend, invent new data processing methods to eliminate it and reprocess the data with the new methods;
6. Repeat Points 4-5 until all understandable physical reasons are eliminated;
7. In case a residual trend is still present in the data, fit the trend and invent an empirical formula to correct for the systematic discrepancies;
8. Document the new processing methods and the empirical fits;

Chopping between the source and 1 or 2 background positions was an ISOPHOT observing mode for faint sources[1]. During the ISO mission more than 7000 observations were performed in this mode. This report presents our results related to the recalibration and reevaluation of observations perfomed in the chopped mode with the C200 detector array. In Section 2 we describe the chopping mode, and provide a statistics for the C200 chopped observations in the ISO Data Archive. Section 3–5 review our processing scheme and the new correction steps. In Section 6 we present an error budget. Our photometric results are summarized in a catalogue which is described in the Appendix.

2 The ISOPHOT chopped observation mode

2.1 Definition of the chopped observing mode

Differential measurements using a chopper are a widespread technique in the infrared astronomy to detect faint sources on top of a fluctuating bright background and to cancel out low-frequency detector noise. Although changes between the telescope and sky background level is negligible for a cold telescope in space, low-frequency detector noise can still appear. In order to avoid latter issue ISOPHOT was equipped with a focal plane chopper which deflected the beam onto adjacent field on the sky[2]. The

[1] In the early phase of the ISO mission chopping was the recommended observing mode for very faint point sources, but later it was replaced by the more efficient mini-map mode in this role.

[2] In the case of reference measurements the beam was deflected onto the two FCSs (Fine Calibration Sources, Laureijs et al., 2003).

modulation frequency of the chopping was adjusted in discrete steps to the brightness of the source. For redundancy reasons a chopper plateau included minimum of four integration ramps (for more details in connection with the data collection strategy of ISOPHOT, see Laureijs et al., 2003), thus for bright sources $f_{chop} = 0.5$ Hz with $n_{ramp} > 4$, while for faint sources $f_{chop} << 0.5$ Hz with $n_{ramp} = 4$.

In the AOTs (Astronomical Observation Template) three different chopper modulation cycles could be selected (for description of saw-tooth, triangular and rectangular modes see Laureijs et al., 2003). However for C200 observations it was only possible to choose rectangular chopping cycle with a single chop throw of $180''$.

2.2 Instrumental effects

Detailed analysis of chopped observations revealed several instrumental effects and some of them make the data evaluation more complicated than expected during the preparation of the mission. In the following we briefly describe these effects and review how relevant are these issues in the case of C200 chopped observations.

2.2.1 Long term detector drifts

Long term detector drifts in the ISOPHOT detectors were already known from the pre-flight laboratory tests. Chopping can successfully eliminate the low-frequency variation if the period of the chopping cycles is significantly shorter than the characteristic timescale of the long term detector drift, and a sufficiently large number of chopper cycles (at least 4 ON-OFF pairs) is executed.

2.2.2 Short term detector transients

Already in the Performance Verification phase, the test measurements demonstrated that chopping between background and source positions causes a periodic change of illumination on the detector which introduces signal transients on the timescale of the length of a chopper plateau. Due to this effect, in general the ON-OFF difference signals extracted from chopped measurements differ from the ones derived in staring mode. Short term signal transients lead to considerable signal loss for P3 and C100 detectors. In the case of C200 detector the signal losses are modest ($\lesssim 15\%$, Acosta&Ábrahám 1998?)

2.2.3 Cosmic glitches

In the case of ISOPHOT measurements cosmic glitches were the main source of random noise. C200 observations also suffered from the effect of glitches. Traditional deglitching processes turned out to be less effective for chopped measurements than for staring ones, because usually only three ramps per chopper plateaux could be used, resulting in poor statistics. The process of pattern analysis (Ábrahám et al., 2003) offers an effective way to eliminate glitches from chopped observations and increases the S/N in chopped measurements.

2.3 Collecting chopped observations from the ISO Data Archive

According to our general scheme in the first step we collected all relevant measurements by searching the ISO Data Archive (IDA) for observations performed with the C200 far-infrared detector using rectangular chopper mode after revolution 93[3]. This search in the IDA resulted in 664 TDT numbers including 1372 measurements.

[3]Between revolution 93 and 94 event occured which changed the radiation characteristic of the main reference source (FCS1). The quality of the FCS calibration is lower for observation before this revolution.

2.4 Identifying secondary photometric standards

As a second step we selected from this database those objects which can be used as primary or secondary standards in the calibration. These objects can be sorted into four different groups:

1. Stars with photospheric templates produced by M. Cohen and P. Hammersley (primary standards).
2. Normal stars with $B-V < 1.3$. For these objects the photospheric flux densities can be predicted from their K- or V-magnitudes (for details see Report I, Moór et al. 2003).
3. Objects for which good quality mini-map photometric data are available.
4. Dedicated observations of some non-stellar objects, which were originally performed to calibrate chopped photometry for C200 detector array.

In Table 1 we present statistics in connection with these groups.

Group	Number of measurements					Total
	C120 [120μm]	C135 [150μm]	C160 [170μm]	C180 [180μm]	C200 [200μm]	
1	3	6	8	9	0	26
2	0	38	0	38	0	76
3	1	3	3	0	5	12
4	4	2	4	0	4	14

Table 1: Statistics about C200 chopped measurements, which can be used as primary or secondary standard

At a first glance the number of measurements of standard objects seems to be satisfactory. However, most of these objects are faint at these wavelengths (F_{pred} or $F_{meas} < 0.1$ Jy).

As it was shown by Kiss et al. (2005) measurements with the C200 detector were confusion noise limited. This statement is especially true for C200 chopped observations where only one background position was measured. We had to take into account this fact when we selected those standard objects which could be detected at least 5σ level at a given wavelength. For chopping measurements cirrus confusion noise estimates are available on the ISO Data Centre home page[4]. According to this condition 28 measurements can be used for the recalibration and validation process.

3 Processing scheme

3.1 ERD→AAP processing with PIA v10.0

From the ERD to the AAP level the data were processed with the PHOT Interactive Analysis software V10.0 (Gabriel et al., 1997).

Table 2 outlines steps at the subsequent processing levels.

After the ERD level we used 8-point patterns of chopper measurements. Generation of patterns is based on the periodicity of the chopped observations. Figure 1 illustrate schematically how to generate a pattern from a chopped measurement. The first 4 point of the pattern are related to the background while the last 4 points are representative of the source position.

Each chopped observation was closed by an internal calibration measurement performed with the last filter used with the current detector. Both FCS1 and FCS2 were measured, where FCS1 was tuned close to the [source+background] power, while FCS2 was set close to the background power as calculated

[4] *http://www.iso.vilspa.esa.es/users/expl_lib/PHT/Quality/cirrus.html*

Processing level	Applied calibration and processing steps
ERD	Ramp Linearization
	Ramp Deglitching (2-threshold method)
	Pattern analysis mode was activated
SRD	Reset Interval Correction
	Dark Current Subtraction
	Signal Linearization
SCP	Calculate responsivities
	Combining pattern signals
AAP	–

Table 2: Applied calibration and processing steps for the C200 chopped observations at the different processing levels of PIA V10.

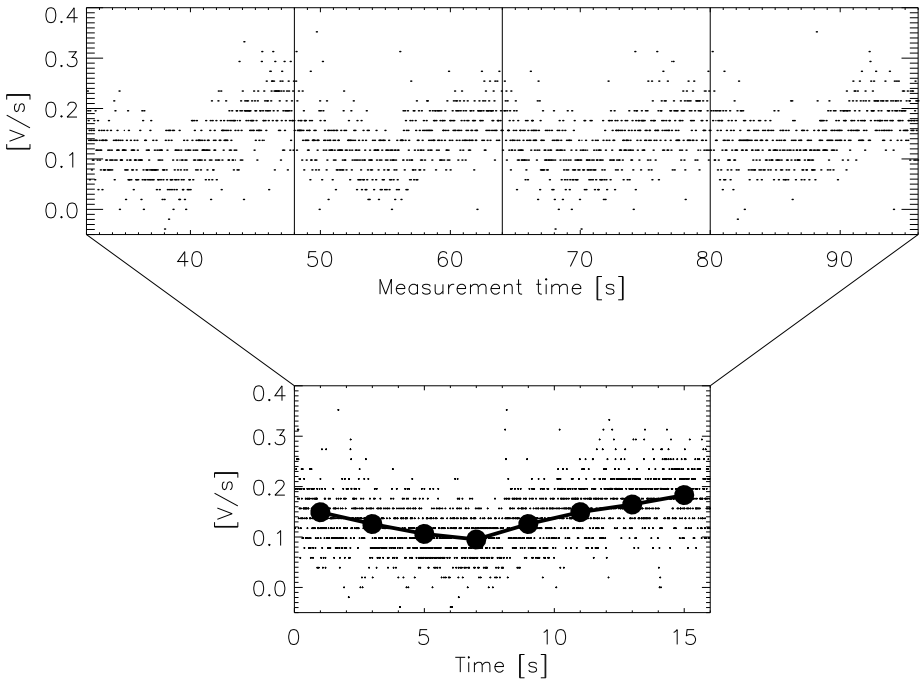

Figure 1: *Schematic view on how to generate a pattern from a chopped measurement. The upper panel displays four chopper cycles of a measurement; each point is a pair-wise difference signal derived from the individual readouts within the ramp. The lower panel demonstrates how the chopper cycles are overplotted and averaged in order to compute the 8 signals of the pattern.*

from the fluxes given by the user. Whenever it was possible we used the FCS1 calibration measurement when we calculated the actual responsivity of the detector at the SCP level.

We followed the general outline of Ábrahám et al. (2003) to extract the final ON-OFF signals from the patterns: (1) the first half of each chopper plateau was discarded; (2) the non-discarded two points of source and of background plateaux was averaged.

Our processing differs from a standard reduction in one step only: empirical signal loss correction was omitted because it caused significant over-corrections in several cases.

3.2 Flux extraction from the AAP

In chopped observations with C200 camera the target was placed on the centre of the array. Thus generally all four pixels detected the source, but only at the pixel corner resulting in decreased signal to noise. Each pixel either at the background and at the source position detects a certain amount of the flux of the source, plus the background assumed to be constant at all positions. Whereas the position of each pixel at each chopping position is determined in image coordinates, the offsets can be calculated easily relative to the position of the source and the footprint fraction factors can be determined from the measured beam profiles. Then the source flux measured by the i^{th} pixel can be derived as:

$$F^i_{meas} = \frac{I^i_s - I^i_{bg}}{f^i_s - f^i_{bg}},$$

where I^i_s and I^i_{bg} are the mean fluxes (in $\frac{\mathrm{Jy}}{\mathrm{beam}}$), while f^i_s and f^i_{bg} are the footprint fractions of the source on the ith pixel at source and at background position.

In a usual C200 chopped observations all four detector pixels observed the source, producing four independent flux density values. The final source flux was derived from the average of these values. Uncertainties were computed from the dispersion of the individual results.

4 Search for systematic trends

4.1 Signal linearization issue

Signal linearization was introduced because responsivities of ISOPHOT detectors were claimed to depend on the illumination level. The magnitude of the effect for the different ISOPHOT detectors, and even for different filters of the same detector was found to be variant (Schulz et al., 2002). In the PIA the signal linearization is performed by interpolation in different lookup tables (related to different detectors and filters) spanning the full range of possible signals.

In order to check the reliability of the signal linearization we plotted the obtained actual responsivities as the function of FCS1 signals measured on different pixels of the C200 detector. In the case of observations which were performed with the C160 filter, we found significant correlation between responsivities and measured signals. On high flux level actual reponsivities turned out to be consistent with default ones. On the other hand on low flux level the actual responsivities deviated from the default responsivities. We fitted the distribution of data points by a polinomial and and use this fit to correct for the systematic deviation from the default response values (corresponding to the high flux end of the curve).

5 Empirical corrections

5.1 Pixel to pixel transformations

After reducing all observations using our standard method – described in the previous sections – we found an obvious non-linear correlation between flux values measured by different pixels of the C200 camera. As a first step we checked for a possible systematic offset between different pixels (hereafter we always take Pix.#3 as reference pixels because its stability). Figure 3 shows histogram of flux differences between Pix.#3 and Pix.#4. We found that the peak of the histogram deviates from zero at 9σ level. Deriving offset values between Pix.#1,2,4 w.r.t Pix#3 per filter, we applied an offset correction on all chopped measurements. In the second step we characterize the possible multiplicative discrepancies. As an example Fig. 4 shows the flux ratio of two pixels ($\frac{F_3}{F_2}$) vs. measured flux. We fit a polinomial to the data points (always keeping Pix.#3 as reference) and corrected C200 chopped measurements with the fitted curve per filter. It is interesting to note that Pix.#2–Pix.#3 show similar behaviour and photometric

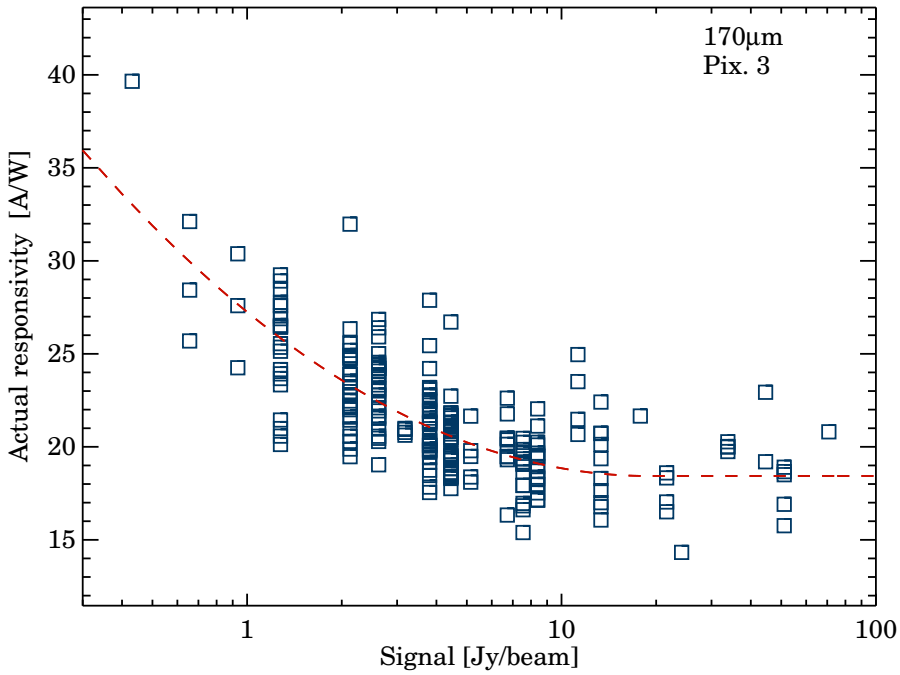

Figure 2: *Plot of responsivities against the FCS1 signals measured through the C160 filter on Pix. 3.*

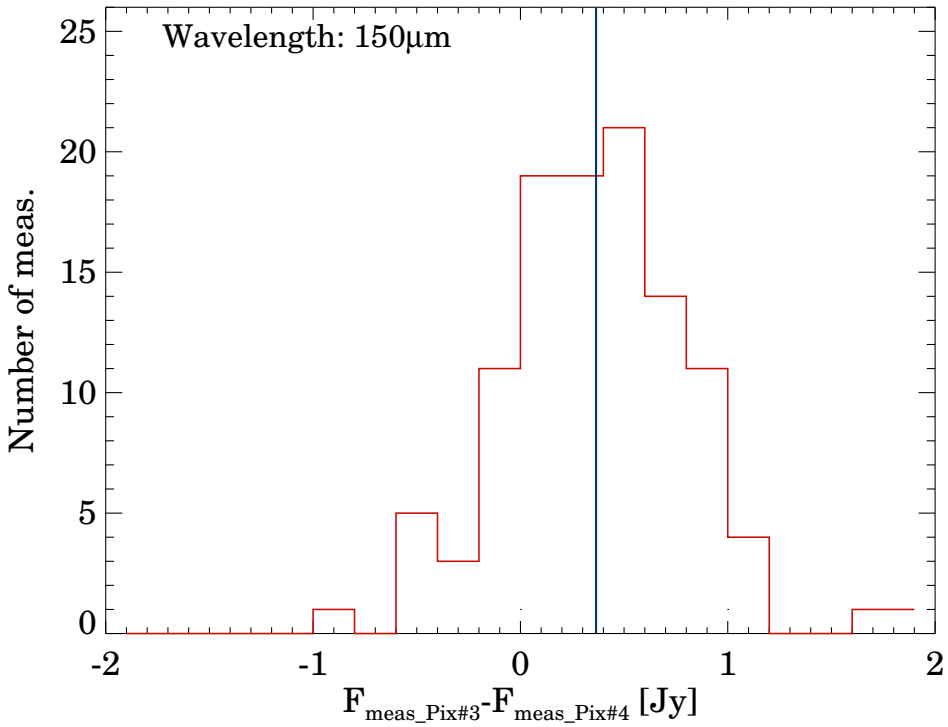

Figure 3: *Histogram of differences between measured fluxes on Pix#3 and Pix#4. Blue line denotes the offset value.*

transformations between these pixels turned out to be practically linear. The same is true for the Pix.#1–Pix.#4 relationship.

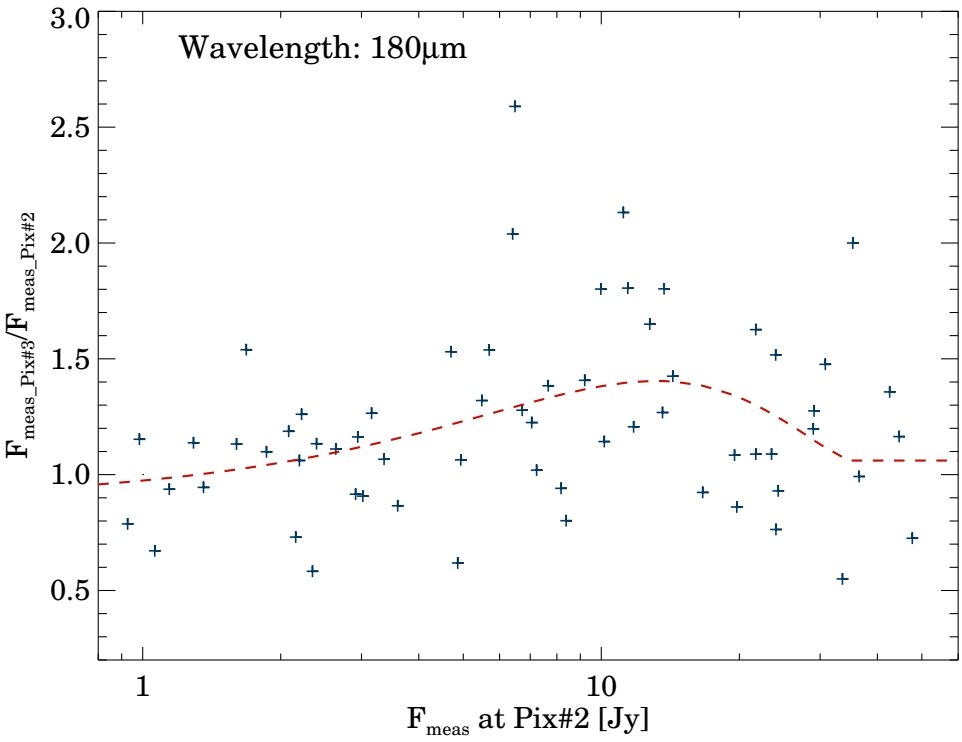

Figure 4: *Ratios of the measured fluxes on Pix#3 to the measured fluxes on Pix#2 vs. the measured fluxes on Pix#2. The correction curve was plotted by red dashed line.*

5.2 Empirical photometric calibration

After transforming the fluxes of Pix.#1,2,4 to the photometric system of Pix.#3 (see previous subsection) we computed the average flux value of the four pixels and their standard deviation. In order to achieve an absolute photometric calibration we compared the resulting fluxes obtained for our secondary standards (subsection 2.4) with their predictions. In these comparison we assumed no filter dependence, and all data point of various filters were plotted together in Fig. 5. We concluded that there is a scaling factor between the measured/predicted flux values and we decided to apply an empirical multiplicative correction of 1.12 on all C200 chopped data. The standard deviation of these data points suggest an absolute calibration accuracy of 20% in the 1–100 Jy flux range. Similar accuracy might be valid for brighter sources as well, but in our analysis we could not check it due to the lack of bright secondary standards.

6 Error budget

6.1 Reproducibility estimate of C200 chopped mode photometry

According to Klaas et al. (2002a) the reproducibility of the different ISOPHOT observing modes were better than the absolute accuracy of the same modes. In order to estimate the reproducibility for the C200 chopped observing mode we evaluated the monitoring sequence of the ISOPHOT standard HR 6705. The standard deviation of the resulting fluxes of the 6 epochs was $\sim$18%. It should be noted however – as suggested by Klaas et al. (2002b) – that part of this scatter is due to variable background (in a chopped measurement the background position depends on the position angle of the focal plane). Thus the true reproducibility value could be lower than quoted above.

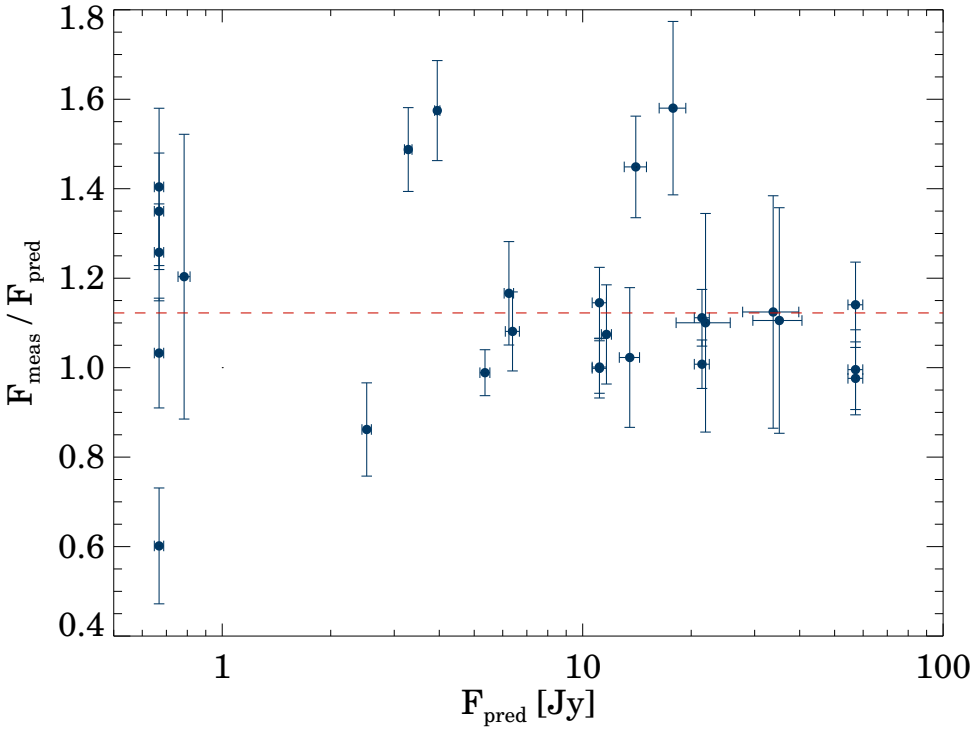

Figure 5: *Measured/predicted flux ratio vs. predicted fluxes for primary and secondary standard objects. Actual responsivities were used in the flux calibration. Dashed line denotes the robust average of the ratios.*

6.2 Photometric accuracy of C200 chopped mode photometry

In order to get an estimate of the typical 1σ uncertainty of C200 chopped measurements we collected all faint source observations ($F_\nu < 2$ Jy) and plotted the histogram of the flux distribution in Fig. 6. The left side of the histogram follows a Gaussian shape while the right side is more asymmetric due to the detection of real sources. We fitted a Gaussian to the left side only and adopted its sigma value of 0.33 Jy as the representative measurement noise of the C200 chopped measurements. Since these value dominated by the confusion noise (see below) in regions of low sky brightness the true flux uncertainties could be lower than this average value.

As was discussed in section 5.2 the absolute calibration accuracy at high flux level ($F_\nu > 2$ Jy) is about 20% derived from our secondary standard ensemble. In the following we assume that this value represents the accuracy of photometric calibration scheme and is also applicable for faint sources. Thus the photometric uncertainties in the catalogue were computed as a quadratic sum of the individual measurement uncertainties and the 20% absolute calibration error.

6.3 Limitations due to cirrus confusion

Spatial fluctuations in the background signal, due to varying cirrus structure or unresolved extragalactic objects give limitation on the detection of faint sources. The sky confusion noise increases generally with increasing separation between the sky and source positions and increasing with larger background surface brightness (Kiss et al., 2005). C200 chopped observations in high surface brightness regions with only one background position and large chopper throw suffered most heavily from this effect. As we noted in section 2.4 in most cases the sky confusion noise dominates the uncertainies of these observations. Estimations of the expected confusion noise for ISOPHOT chopped measurements are available on the ISO Data Centre home page (see section 2.4). Comparing our individual uncertainties with the expected

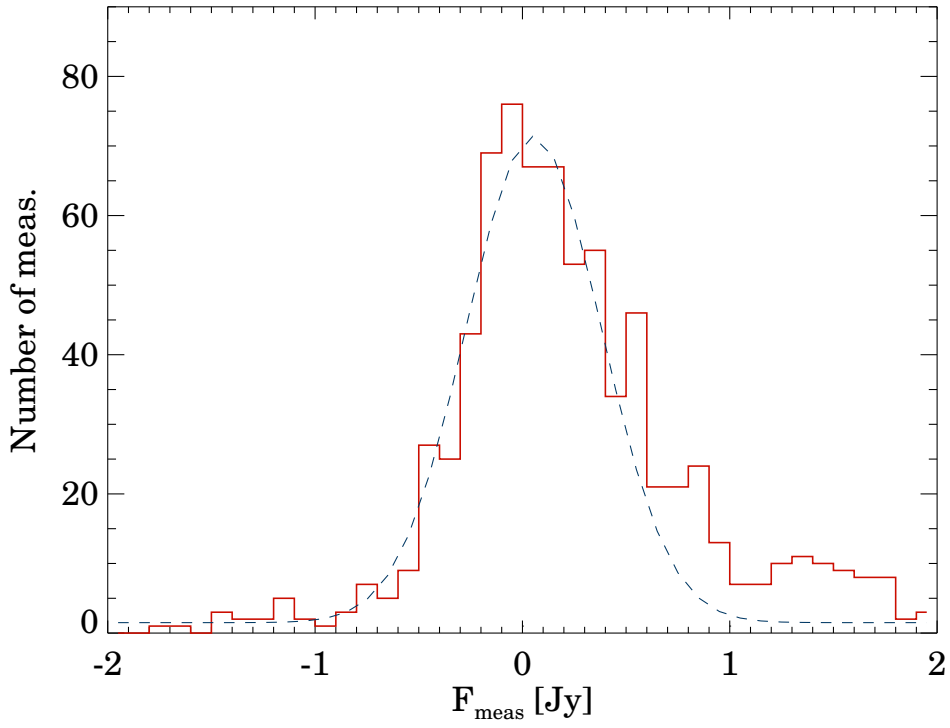

Figure 6: *Histogram of the measured fluxes for C200 chopped observations. The low flux part of the histogram (the left hand side of the flux distribution) is assigned to non-detections and fitted with Gaussian in order to estimate the 1σ uncertainty of C200 chopped measurements. The dashed curve is a Gauss curve with average* $m = 0.04\,Jy$ *and dispersion* $\sigma = 0.33\,Jy$.

confusion noise a number of cases were found when the individual measurement was significantly lower than the confusion noise. We think that in these situations the measurement noise was underestimated (it was computed as the standard deviation of the four pixels of the C200 array, which is a low number statistics). As a conservative way for determining the final photometric uncertainties in the catalogue, we selected those cases when the measurement error was less than 50% of the confusion noise and replaced the formal flux error with the latter value. We note that our typical measurement errors are comparable with those of the IRAS 100μm observations in the PSC (Point Source Catalogue).

References

Ábrahám, P., Acosta-Pulido, J. A., Klaas, U., Bianchi, S., Radovich, M., Schmidtobreick, L., 'The calibration legacy of the ISO Mission', proceedings of a conference held Feb 5-9, 2001. Edited by L. Metcalfe, A. Salama, S.B. Peschke and M.F. Kessler. Published as ESA Publications Series, ESA SP-481. European Space Agency, 2003, p. 89.

Gabriel C., 1997, in Proc. of the ADASS VI conference (Eds.: G. Hunt, H.E. Payne, ASP Conf.Ser. 125), 108

Kiss, Cs., Klaas, U., Lemke, D., 2005, A&A 430, 343

Klaas U. et al., 2002, "ISOPHOT Calibration Accuracies (Version 5.0)"

Klaas, U., & Richards, P. "Report on the Scientific Validation of the PHT OLP Version 10.0"

Laureijs, R. J., Klaas, U., Richards, P. J., Schulz, B., & Ábrahám, P. 2003, The ISO Handbook Vol. IV.: PHT - The Imaging Photo-Polarimeter, Version 2.0.1, ESA SP-1262, European Space Agency

Moór, A., Ábrahám, P., Kiss, Cs., Csizmadia, Sz., 2003, Far-infrared observations of normal stars measured with ISOPHOT in mini-map mode (http://pma.iso.vilspa.esa.es:8080/hpdp/techn ical_reports/technote5.pdf)

Schulz, B., Huth, S., Laureijs, R. J., et al. 2002, A&A, 381, 1110

Appendix: description of the catalogue

The flux densities for C200 chopped measurements resulted from recalibration described in this document were listed in a photometric catalogue which is included as Highly Processed Data Product. In the following we described the fields of the catalogue. We note that several observations were excluded from the catalogue due to different technical reasons.

Column	Field	Unit	Description
(1)	Object name		SIMBAD compatible name. Filled if a compact source from SIMBAD can be associated with the ISOPHOT target without doubt.
(2)	Object type		Standard SIMBAD code for object type.
(3)	ISO name		Target name as given by the original ISO proposer.
(4)	TDTNUM_ON		The 8-digit TDTNUM of the on-source observation.
(5)	On_ Meas.		Index of the on-source measurement within TDTNUM_ON.
(6)	RA(2000)		RAh, RAm, RAs of the ISOPHOT position.
(7)	Dec(2000)		DECd, DECm, DECs of the ISOPHOT position.
(8)	Detector		ISOPHOT detector.
(9)	Wavelength	[μm]	Nominal wavelength of the ISOPHOT filter.
(10)	Aperture	[arcsec]	Square aperture for C200 detector.
(11)	Epoch		Epoch of the observation.
(12)	TDTNUM_ OFF		The 8-digit TDTNUM of the off-source observation.
(13)	Off_Meas.		Index of the off-source measurement within TDTNUM_OFF.
(14)	Flux density	[Jy]	Flux density of the source. No colour correction applied.
(15)	Flux uncertainty	[Jy]	Flux uncertainty. No colour correction applied.
(16)	Quality		Quality of the observation. R1 – Standard processing according to the scheme described in the report. R2 – Observation was carried out at the very beginning or at the very end of orbit. Reduced photometric reliability at orbital phase lesser than 0.2 or greater than 0.8. R3 – Measured flux was out of the empirically calibrated range. R4 – Default FCS is used.

Table 3: Description of the catalogue